A Global Study of Ridge Belt Morphology and Morphometry on Venus. Zachary W. Williams[1], Paul K. Byrne[1], Jeffrey A. Balcerski[2], and DelWayne Bohnenstiehl[1]. [1]Planetary Research Group, North Carolina State University, Raleigh, NC 27695 (zwwillia@ncsu.edu), [2]Ohio Aerospace Institute, Cleveland, OH 44142.

Introduction: The surface of Venus hosts globally distributed, linear, positive-relief systems of shortening structures, termed ridge belts in the literature [1–7]. Previous studies concluded that ridge belts are surface expressions of spatially concentrated crustal shortening accommodated by thrust faulting and folding [1–7]. Despite assessment in previous studies [1–6], the morphological characteristics of these globally distributed systems have yet to be fully described and catalogued. With the recent availability of regional topographic data at resolutions greater than the Magellan altimetry dataset [8], it is now possible to gain a more comprehensive understanding of the morphological properties of these shortening systems.

Here, we aim to acquire detailed morphometric data for a globally distributed set of ridge belts. With these more robust morphologic parameters established, we mapped observable tectonic structures—faults and folds—within a subset of those selected ridge belts. We then used topographic profiles and relief values from the collected morphometric data to acquire local estimates for the effective elastic thickness of the lithosphere, evidenced by flexural signatures in topography proximal to these ridge belts.

Data and Methods: We utilized global Magellan synthetic aperture radar full-resolution radar map (SAR FMAP) 75-meter-per-pixel (m/px) left- and right-look mosaics for the initial identification of candidate ridge belts. For topographic measurements, we used stereo-derived digital elevation models (DEMs) produced by Herrick et al. [8], which offer ~20% global coverage at 1–3 km/px resolution.

Morphometric Data Extraction: We conducted a global survey with ArcGIS to identify ridge belts on the basis of morphological descriptions from existing studies [e.g., 1, 4–7, 9]. This survey yielded 398 discrete landforms as potential study ridges. We downselected 24 candidates for further analysis that have a well preserved morphology (i.e., not bisected by craters, buried by volcanism, or destroyed by subsequent tectonism) and are not obviously kinematically associated with neighboring systems. Of these 24 structures, 12 are within the Herrick DEM coverage [8]. Outlines of the selected ridge belts were manually traced and recorded within ArcGIS. We developed a Python routine to automatically record the strike of each landform from the mapped outline, and to take width measurements (representing the distance across strike to opposing boundaries of the landform) at regular intervals along the structure, orthogonal to the strike at the point of collection (**Fig 1a)**. For those ridges covered by the Herrick DEMs, we extracted cross-sectional profiles at each point where we recorded a width measurement.

Fault Mapping: Individual tectonic structures within the selected ridge belts were mapped for seven of the selected ridge belts. These seven were selected on the basis of their orientation relative to the look directions of the Magellan radar, and the availability of both left- and right-look SAR data. Identification and mapping of faults was conducted using the left- and right-look SAR survey global mosaics at 1:200,000 view scale. Assuming a similar surface mineralogy across the ridge belts, the variation in backscatter (the value gathered by SAR) is a function of surface roughness and incidence angle [10]. Mapped faults were classified as either extensional or shortening (**Fig 2a**). On the basis of comparison with tectonic structures on Earth and other rocky bodies, we interpreted arcuate fault traces as denoting shortening structures (likely folds atop thrust faults) [11]. The arcuate aspect of these traces gives the vergence of the overlying fold, an asymmetry in the fold shape that gives the direction of tectonic transport and thus the down-dip direction for each mapped thrust fault. Linear fault traces, commonly offset in an *en echelon* manner, were taken to correspond to normal faults (**Fig. 2b**).

Lithospheric Flexure: Additional cross-sectional profiles were drawn along width measurements at twice the horizontal extent of the original profiles. This was done to capture any topographic signal associated with the flexure of the elastic lithosphere in response to the mass of the ridge belt, which would represent a line load, akin to a seamount chain [12]. Upon examining the extended profiles, four of the selected ridge belts displayed evidence of lithospheric flexure as resolved by the Herrick DEM data [8] (**Fig 3)**. The solution to the topographic response to a line load (represented as a point load on a 1-dimensional profile), *w*, is given by the dampened sinusoidal function [12]:

$$w = w_0 e^{-\frac{x}{a}}\left(\cos\left(\frac{x}{a}\right) + \sin\left(\frac{x}{a}\right)\right), \qquad [1]$$

where w_0 is the maximum amplitude of flexure along the breadth of the profile, *x*, with respect to the flexural parameter, *a*, given by the relation:

$$a = \sqrt[4]{\frac{4D}{(\rho_m - \rho_i)g}}, \qquad [2]$$

where *D* is the flexural rigidity, $\rho_m - \rho_i$ is the difference between mantle and atmospheric density, and g is the acceleration due to gravity. Flexural rigidity is given by

$$D = \frac{E}{12(1-\nu^2)}h^3, \qquad [3]$$

where *E* is Young's modulus, *v* is Poisson's ratio, and *h* is the depth of the elastic lithosphere. Values for Young's modulus and Poisson's ratio for anhydrous basalt, and density contrast across the lithosphere, were taken from previous studies of lithospheric flexure on Venus [13]. The depth of the elastic lithosphere was determined using a least-squares optimization of a cost function for the set of equations using a simplex method, with *h* and w_0 as two of the free parameters.

Results and Discussion: *Morphometric Analysis*: Values for strike, width, and location for all 24 structures were extracted from the global SAR FMAP (**Fig. 1a**). The average width of the 24 ridge belts we selected is 81 km (with a maximum width value of 207 km, a minimum width of 9 km, and a median value of 78 km). The standard deviation of width measurements within each ridge belt ranged from 59 to 4 km (with an average value of 19 km and median of 14 km for all 24 structures). We found no evidence for regional or global trends in the orientation of the selected ridge belts, with values distributed across the full range of possible strikes. Average relief values were determined from the full set of cross-sectional profiles for each of the ridges within the subset of DEM-covered ridge belts (**Fig. 1b**). For these 12 structures, we found an average relief value of 597 m and a median value of 551 m (with maximum and minimum values of 938 m and 232 m, respectively). Cross-sectional profiles of the ridge belts uniformly display an observable fore- and back-limb morphology consistent with thrust-fault-related landforms (**Fig 1b**).

Fault analysis: Our preliminary mapping of the ridge shown in **Fig. 2** indicates that tectonic structures within the ridge belts are predominately thrust faults and their related folds (**Fig 2b)**. Of the 455 thrust fault traces we mapped in the ridge, 77% appear to dip to the east. This tectonic transport direction (i.e., to the west), agrees with that suggested by the overall cross-sectional profile of the ridge itself.

Lithospheric Flexure: Preliminary estimates of the depth of the elastic lithospheric give values of 13–25 km (**Fig 3**), largely consistent with previous studies for the planet's lowlands [e.g. 14–16]. Furthermore, this result agrees with predictions of yield strength envelopes that suggest a relatively thin elastic lithosphere as a function of the high surface temperature [17]. This inference can be further tested with forward modeling of ridge belt morphology [18].

References: [1] Frank, S. L. and Head, J. W. III. (1990) *Earth, Moon, and Planets.* [2] Ivanov, M. A. and Head, J. W (2013) *Planetary and Space Science, 84.* [3] Barsukov, V. L. et al. (1986) *JGR, 91.* [4] McGill, G. E. and Campbell, B. A. (2006) *JGR, 111.* [5] Ivanov, M. A. and Head, J. W. (2011) *Planetary and Space Science, 59.* [6] Solomon, S. C. et al. (1992) *JGR, 97.* [7] Basilevsky, A. T. and Head, J. W. (2003) *Report on Progress in Physics, 66.* [8] Herrick, R. R. et al. (2012) *EOS, 93, No. 12.* [9] Balcerski, J. A. and Byrne, P. K. (2018) *LPSC 2018,* abstract 2083. [10] Farr, T. G. (1993) *Guide to Magellan Image Interpretation.* [11] Burg, JP. (2017) *Tectonics: Thrust Systems.* [12] Lowrie, W. (2007) *Fundamentals of Geophysics.* [13] O'Rourke, J. G. and Smrekar, S. E. (2018) *JGR, 123.* [14] Anderson, F. S. and Smrekar, S. E. (2006) *JGR, 111.* [15] James, P.B. et al. (2012) *JGR, 118.*[16] Buck, W.R. (1992) *Geophysical Research Letters, 19.* [17] Ghail, R. (2015) *Planetary and Space Science, 113-114.* [18] Balcerski, J. A. and Byrne, P. K. (2018) *VEXAG 2018,* abstract 2137.

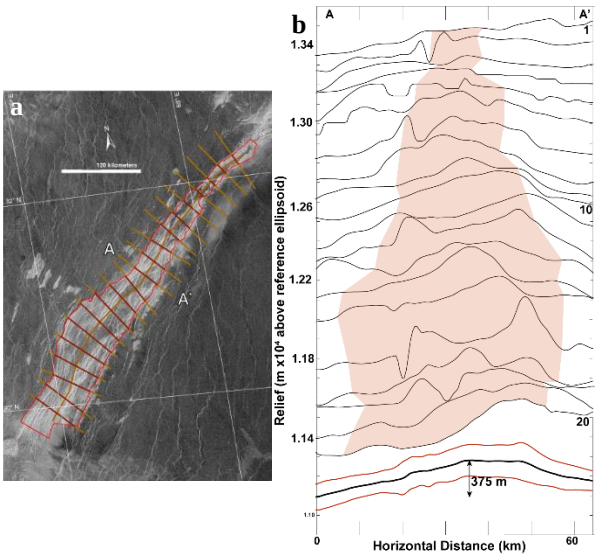

Fig. 1a. An example of structural mapping and data extraction for a ridge belt centered at 30.8° N, 66.8° E. Width measurements (burgundy lines) and cross-sectional profiles (orange lines) are shown. **b.** Cross-sectional profiles of the ridge; the solid black line is the average of 20 extracted profiles (light grey).The shaded orange regions indicate the mapped extent of the ridge belt. This structure's relief is 386m, with a standard deviation of 105 m.

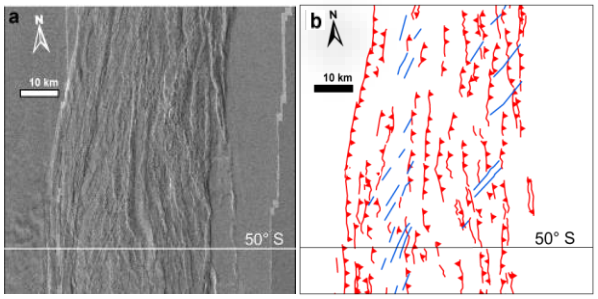

Fig. 2a. An example of overlain left- and right-look SAR data used to map fault traces within a ridge belt system centered at 49° S, 27° E. **b.** Mapped fault traces within the SAR data. Red fault traces are designated thrusts, with teeth indicating the down-dip direction; blue traces are normal faults.

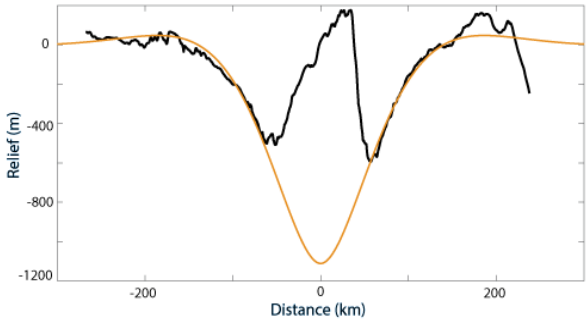

Fig 3. An example result of a least-squares optimized fit to the observed topographic response of the Venus lithosphere to a ridge belt centered at 3° S, 22° W. Results from this model indicate an elastic lithosphere thickness of 21 km.